# Role of temperature on nonlinear cardiac dynamics

Flavio H. Fenton, Alessio Gizzi, Christian Cherubini, Nicola Pomella, and Simonetta Filippi

# The role of temperature on nonlinear cardiac dynamics

Flavio H. Fenton[1], Alessio Gizzi[2,3], Christian Cherubini[2,4], Nicola Pomella[2,3] and Simonetta Filippi[2,4],

[1] *School of Physics, Georgia Institute of technology, Atlanta, GA 30332, USA*
[2] *Nonlinear Physics and Mathematical Modeling Laboratory,*
*University Campus Bio-Medico of Rome, I-00128, Rome, Italy*
[3] *Alberto Sordi Foundation, Research Institute for Aging, I-00128, Rome, Italy and*
[4] *International Center for Relativistic Astrophysics - I.C.R.A.*
*University of Rome "La Sapienza", I-00185 Rome, Italy.*

Thermal effects affecting spatio-temporal behavior of cardiac tissue are discussed by relating temperature variations to pro-arrhythmic dynamics in the heart. By introducing a thermo-electric coupling in a minimal model of cardiac tissue, we are able to reproduce experimentally measured dynamics obtained simultaneously from epicardial and endocardial canine right ventricles at different temperatures. A quantitative description of emergent pro-arrhythmic properties of restitution, conduction velocity and alternans regimes as a function of temperature is presented. Complex discordant alternans patterns that enhance tissue dispersion consisting of one wave front and three wave backs are described in both simulations and experiments. Possible implications for model generalization are finally discussed.

## I. INTRODUCTION

Excitable media are systems which allow the propagation of solitary excitation waves without damping. One of the most striking characteristics of these systems is the possibility to support rotating spiral waves [1–3]. In cardiology these have been experimentally observed and associated to irregular rhythms such as tachycardia and fibrillation [4, 5]. Thermal effects on chemical excitable media and biological tissues, are important and can have large effects in the development of these arrhythmias starting from the dynamics of a single spiral wave [6]. Humans and animals have normally a systemic temperature which is kept approximately constant through many delicate physiological feedbacks. When temperature changes occur because of pathological conditions, as in case of fever or inflammation, it is well known that nervous and cardiac systems result affected [7]. For example, when the body core temperature is raised because of sport fatigue or heat strokes up to the extreme measured cases of more than 42°C (hyperthermia) [8], serious dysfunctions in brain and heart do occur (in some cases, this could be a possible cause for sudden death in sports). On the other hand, when body temperature is lowered to 26°C or less (hypothermia) because of surgery or therapeutical procedures [9] or for unfortunate events as shipwrecks or avalanches [10–13], death for fibrillation as well as brain damages are well known to occur [14].

Temperature can strikingly affect many electrophysiological characteristics of nerves and cardiac tissues, as action potential (AP) amplitude, duration and conduction velocity [15–17]. In fact, many experimental studies of alternans, a dynamical period doubling instability that develops during fast pacing and enhances dispersion of repolarization and thus is known to be pro-arrhythmic [18–20], have used low temperatures to enhance and analyze the dynamical regions for alternans. Recently, new experimental evidences on heat transfer in extended sections of biological media have further shown the importance of considering directionality in the diffusivities due to tissue anisotropy and vascularization [21, 22]. These are all not unexpected results: excitable cells can be seen as idealized electrical circuits, where resistances and conductances are known by classical electromagnetics to be affected by temperature changes. In the field of heat transfer in biological systems, a cornerstone is represented by the classical work of Hodgkin and Huxley on nerve action potential [23] in which a simultaneous experimental and mathematical study of a biological nonlinear system was presented for different axonal constant temperature baths.

From a modeling point of view, excitable media and thus the electrical dynamics of cardiac cells can be well described by systems of differential equations of Reaction-Diffusion (RD) type [24, 25]. In these studies the electromechanical feedback can be included in order to account for tissue conduction [26–29] while the simplest way to include temperature in such a mathematical formalism, is to adopt a chemical thermodynamic approach, i.e. van't Hoff and Arrhenius equations [30] together with Pennes bioheat transfer equation [31, 32]. In cardiac dynamics Literature few studies exist, most of them of theoretical nature, showing how temperature affects action potential nonlinear dynamics [33–35] and current models do not reproduce well the experimentally observed changes [36].

Such a gap is partially filled in this work. Here we specifically present both an experimental and theoretical study to analyze the effect of temperature on averaged cardiac restitution curves and alternans dynamics. We synchronously recorded the endocardial and epicardial action potential signals via optical mapping on whole right ventricular canine hearts perfused at different temperatures. We introduce then the above aforemen-

tioned thermo-electric coupling in a minimal cardiac electrophysiological mathematical model, whose parameters have been fine tuned on humans [37]. We qualitatively and quantitatively reproduce the experimental results by introducing two thermal contributions in the model previously adopted for axonal experiments: a modification of (i) the rates of changes of the gating variables, through an effective $Q_{10}$ factor (following an Arrhenius' law), and a modification of (ii) the ionic currents, in accord with Moore's experiments [38]. We study the dynamics in space by simulating the model in one dimensional cables and rings of cardiac cells [39, 40], on the lines of standard physiology studies on reentry circuits in Cardiology. Such an analysis allows us to investigate emergent phenomena associated with alternans and conduction blocks from a dynamical system point of view by using bifurcation diagrams.

The paper is organized as follows. In Sec. II we introduce the mathematical model adopted. In Sec. III we compare the experimental measurements with the modeled predictions, highlighting the alternans behavior. In Sec. IV we critically discuss the model, proposing further developments and applications.

## II. MODELING

Although the level of ionic models complexity has increased significantly in the last decades [24], in this work we have adopted a four-variable minimal phenomenological model (MM) for cardiac action potential propagation [37]. Such a choice allows us to set the minimal level of complexity, but at the same time permits to track the relevant parameters necessary to correctly reproduce the experimental cardiac action potential restitution properties and alternans dynamics here synchronously recorded for both the endocardium (ENDO) and epicardium (EPI) layers. Model equations are:

$$\partial_t u = D\nabla^2 u - (J_{fi} + J_{so} + J_{si}) \tag{1}$$

$$\partial_t v = \phi_v(T)\left[(1 - H(u - \theta_v))\frac{(v_\infty - v)}{\tau_v^-} - \frac{H(u - \theta_v)v}{\tau_v^+}\right] \tag{2}$$

$$\partial_t w = \phi_w(T)\left[(1 - H(u - \theta_w))\frac{(w_\infty - w)}{\tau_w^-} - \frac{H(u - \theta_w)w}{\tau_w^+}\right] \tag{3}$$

$$\partial_t s = \phi_s(T)\left[\frac{(1 + \tanh(k_s(u - u_s)))/2 - s}{\tau_s}\right], \tag{4}$$

where the ionic density currents are

$$J_{fi} = \eta_{fi}(T)\left[-H(u - \theta_v)(u - \theta_v)(u_u - u)\frac{v}{\tau_{fi}}\right] \tag{5}$$

$$J_{so} = \eta_{so}(T)\left[(1 - H(u - \theta_w))\frac{(u - u_o)}{\tau_o} + \frac{H(u - \theta_w)}{\tau_{so}}\right] \tag{6}$$

$$J_{si} = \eta_{si}(T)\left[-H(u - \theta_w)\frac{ws}{\tau_{si}}\right], \tag{7}$$

and the voltage-dependent time constants

$$\tau_v^-(u) = (1 - H(u - \theta_v^-))\tau_{v1}^- + H(u - \theta_v^-)\tau_{v2}^- \tag{8}$$

$$\tau_w^+(u) = \tau_{w1}^+ + (\tau_{w2}^+ - \tau_{w1}^+)\frac{\tanh(k_w^+(u - u_w^+)) + 1}{2} \tag{9}$$

$$\tau_w^-(u) = \tau_{w1}^- + (\tau_{w2}^- - \tau_{w1}^-)\frac{\tanh(k_w^-(u - u_w^-)) + 1}{2} \tag{10}$$

$$\tau_{so}(u) = \tau_{so1} + (\tau_{so2} - \tau_{so1})\frac{\tanh(k_{so}(u - u_{so})) + 1}{2} \tag{11}$$

$$\tau_s(u) = (1 - H(u - \theta_w))\tau_{s1} + H(u - \theta_w)\tau_{s2} \tag{12}$$

$$\tau_o(u) = (1 - H(u - \theta_o))\tau_{o1} + H(u - \theta_o)\tau_{o2}. \tag{13}$$

Here $H(x)$ represents the standard Heaviside step function; $u$ is the dimensionless membrane potential, rescaled to dimensions of $mV$ by using the map $V_m = (85.7u - 84)\, mV$; while $v$, $w$ and $s$ are the three local gating variables. In the formulation here proposed the time constant $\tau_w^+(u)$ (Eq. 9) has been considered as an hyperbolic function of the voltage membrane, with respect to the original model [37], in order to better match the experimental restitution curves given in the following. Finally, the asymptotic values are given by

$$v_\infty = \begin{cases} 1, & u < \theta_v^- \\ 0, & u \geq \theta_v^- \end{cases} \tag{14}$$

$$w_\infty = (1 - H(u - \theta_o))(1 - \frac{u}{\tau_{w\infty}}) + H(u - \theta_o)w_\infty^*, \tag{15}$$

and the temperature dependent factors are expressed by

$$\phi(T) = Q_{10}^{(T - T_a)/10} \tag{16}$$

$$\eta(T) = A(1 + B(T - T_a)). \tag{17}$$

These two additional contributions affect the kinetics of the gating variables and the time constants of the ionic currents, respectively. Their variation with respect to temperature is reported in Fig. 1, in which the $Q_{10}$, $A$ and $B$ coefficients are physiologically based [16, 33] ($T_a = 37°C$ represents the tissue reference temperature), and fine tuned in order to reproduce the synchronously measured action potential shapes, restitution curves and conduction velocities for both the endocardial and the epicardial surfaces.

*a. Experimental Protocol.* All experimental procedures were approved by the Institutional Animal Care and Use Committee of the Center for Animal Resources and Education at Cornell University. The tissue preparation has been previously described [5, 41]. Adult beagle dogs of either sex were anesthetized with Fatal-Plus, and their hearts were rapidly excised via a left thoracotomy and placed in cold, aerated normal Tyrode solution. The right coronary artery was cannulated with polyethylene tubing, and the right ventricular myocardium was excised and suspended in a heated transparent tissue Plexiglas chamber. It was both perfused and superfused with normal Tyrode solution by that artery. After 20 minutes of equilibration at physiological temperature ($37.0\pm0.5°C$), the preparation was stained with the voltage-sensitive dye Di-4-ANEPPS. Blebbistatin was added to prevent motion artifact over the first 40 minutes. A total of N=6

right ventricular preparations were studied. Right ventricles (RV) were laid flat on a bath (that was kept at the same temperature as the perfused Tyrode solution) so simultaneous recordings of the electrical activity on the epicardium and endocardium could be performed. Stimulation was induce by a bipolar electrode situated at the edge of either the posterior or anterior free wall, so activations originated almost simultaneously at the epicardium and endocardium, and the wave propagated perpendicular to the thickness of the tissue.

The optical mapping setup has been described previously [42]. Briefly, illumination was provided by high-performance light-emitting diodes driven by a low-noise constant-current source. The illumination efficiency was significantly enhanced by collimator lenses. The epicardium and endocardium were imaged simultaneously using two synchronized cameras. The fluorescence emission light was collected for each camera by a Navitar lens, passed through a long-pass filter ($< 610 \, nm$), and imaged by a $128 \times 128$ back-illuminated electron-multiplied charge-coupled device array with a high quantum efficiency (peak QE $> 90\%$). The signal was digitized with a 16-bit analog/digital converter at a frame rate of $511 \, Hz$ with a spatial resolution of $600 \, \mu m$ per pixel for a grid size of $7.7 \, cm \times 7.7 \, cm$.

We experimentally measured dynamic action potential duration (APD) restitution curves by pacing the tissue at twice diastolic threshold current pulses. Pacing cycle length (CL) was applied starting from high CL (typically $1000 \, ms$ or higher) and decreasing in $50 \, ms$ decrements until reaching $250 \, ms$, after which the CL was shortened in $10 \, ms$ decrements until capture was lost or ventricular fibrillation was induced. Such a procedure ensures that no alternans is present in the tissue at the starting point of the restitution curve. At each CL, pacing was applied for at least 1 minute before recording to ensure that steady state was reached, then recordings were made for 5 seconds, or more, at each CL. Data were analyzed with a custom-built interactive Java program. Data were processed to remove signal drift and fluorescence noise; normalization was conducted on a pixel-by-pixel basis and the time averages of length 7 (3 forward and 3 backward) and weighted Gaussian space averages (8 neighbor pixels) of the signal were performed. Pixels not visualizing the tissue were removed by an user define mask. Optical APD and diastolic interval (DI) were measured at 25% repolarization threshold ($APD_{75}$) obtained using standard linear interpolation [43]. The relation between these quantities simply reads: $CL = APD + DI$.

The alternating regime was defined by computing the difference between two consecutive APDs for every recorded pixel on the tissue, thus applying the following rule:

$$
\begin{aligned}
\Delta APD(x,y)_n &= APD(x,y)_n - APD(x,y)_{n-1} \rightarrow \\
&\rightarrow \begin{cases} |\Delta APD(x,y)_n| > 2 \, ms & Alternans \\ |\Delta APD(x,y)_n| \leq 2 \, ms & Node \end{cases}
\end{aligned} \quad (18)
$$

where $n \geq 2$ denotes the beat number and $APD(x,y)$ is the duration of the action potential at a pixel in position $(x,y)$ in the 2D mapped field. Such a definition allows us to consider the recording temporal resolution of $2 \, ms$ inside the difference range of $4 \, ms$ and to define the tissue as non-alternating (Node) when $\Delta APD(x,y)$ was greater than $-2$ and less than $+2 \, ms$, and as alternating otherwise.

The local conduction velocity (CV) was measured in the direction of the propagation wave only using the distributions of activation maps (see Fig. 4), thus minimizing the effects of curvature [44, 45] on the measured value. Optical mapping techniques for synchronous dual cardiac AP wave recordings have been widely validated [46] and the measurements here performed are in line with other works (see Sec. III).

*b. Numerical Simulations.* Numerical simulations were solved on a one dimensional cable or a ring via the forward Euler method with $dx = 0.025 \, cm$ and $dt = 0.1 \, ms$. This choice, has been shown to give resolved solutions and is in line with several previous works [39, 40, 47] and for the aims of the present study, allows us to consider diffusion effects, to study propagating waves and to evaluate conduction velocities other than alternans dynamics in a minimal computational domain. Numerical convergence was ensured by a careful control of the conduction velocity depending on the spatial discretization adopted (see [48] for details). The modeled restitution curves and conduction velocities were calculated following a protocol similar to the experimental one.

## III. RESULTS

While the MM model was constructed for normal physiological temperature, i.e. 37°C, we found that by including Eq. 16 and 17, into the model, the modified equations on a 1D cable are able to reproduce most of the experimental cardiac characters at different temperatures in agreement with previous experimental evidences obtained in different tissues and with different experimental techniques [15]. In the following we characterize the complex phenomena observed experimentally with the phenomenological model.

### A. AP Shapes & Restitutions

In Fig. 2 (left) we compare experimental and modeled AP shapes from endocardial and epicardial surfaces. We observed (i) the decrease of AP amplitude and (ii) the lengthening of APD for both surfaces, together with (iii) the enhancement of the spike and dome phase for the EPI signals as temperature decreases. These behaviors are due to slowing of the sodium and calcium dynamics at lower temperatures. The model shows faster upstrokes than experimental signals due to the optical mapping technique, which induces a signal smoothing due to the

time resolution ($2\,ms$). However, the main quantities are recovered with good accuracy as discussed below.

In Fig. 2 (right) experimental and modeled restitution curves are compared. The curves are averaged between two consecutive APDs, therefore we do not consider the experimental nor the modeling splitting of the restitutions [49]. (i) Qualitative and quantitative matching of the modeled trends are obtained in the thermal range from 29°C to 40°C (fitting the temperatures 29, 33, 37 and 40°C). A steepness quantification of the curves is reported in the figure caption showing as the maximum CL at which the slope is $\geq 1$ increases for colder thermal baths. The model without any modification other than the thermo-electric coupling successfully produces a quick loss of plateau for short pacing periods, resulting in very small AP durations as in the experimental data. (ii) The sigmoidal shape slope of the restitution curves at $T = 26$°C requires an *ad hoc* set of parameters in order to be reproduced by the model. This is mainly due to the definition of the $Q_{10}$ factors, which are rigorously valid in a thermal range of 10 degrees. The complete set of parameters for the two cases are reported in Tab.1. In our model tuning we modified the set of parameters with a minimal variation of the thermal coefficients, $Q_{10}$, $A$ and $B$.

In Fig. 3 we further compare the restitution curves synchronously recorded on the opposite surfaces for the different temperatures tested. In general we observe that: (1) the ENDO restitution is always higher than the EPI one, meaning that the corresponding action potentials are larger at every CL; (2) the two curves assume a maximum difference for the highest CL and tend to shrink when approaching the conduction block CL in the thermal range from 33°C to 40°C, as enhances by the differences of the fitted APD values (gray bars); (3) for $T = 26, 29$°C a measurable deviation from monotonicity is visible, and a local maximum in their difference can be measured in the region of slope changing; (4) however at lower temperatures the restitution curves tend to remain parallel, even if sigmoidal. In Fig. 3 (F) the maximum APD differences for the five cases are summarized for the highest and lowest CLs, together with two intermediate cases at $T = 26, 29$°C. Such a behavior highlights the strongly nonlinear effect of temperature on the collective tissue dynamics between the two surfaces separated by a wall thickness that is less or equal to about $1\,cm$ at the thickness section, much smaller than the surface dimensions. The reduction/enhancement of the depolarization gradients at higher/lower temperatures, respectively, due to the fastening/slowing of the transmembrane currents, and the effects of anisotropy, are the main ingredients for the explanation of the observed phenomena.

The fitting curves of the experimental restitution values, plotted in the thermal range from 26°C to 40°C, are polynomial or piecewise interpolating functions of the diastolic interval, i.e. $APD = APD(DI)$. Complete expressions, parameters and correlation percentages are reported in appendix and in Tab. 2 and 3.

## B.  CV, Alternans Onset & Conduction Block

In Fig. 4 (Top left) we compare experimental and modeled conduction velocities, for the constant maximum imposed CL, observing a monotone CV decrease as temperature decreases for both surfaces. The slowing of the sodium conductance and time constants reduces the CV in the model in a similar way as the experimentally measured velocities. However, as indicated by the error bars, there is no significative difference between the two surfaces. The CV similarity is further appreciated by the two sequences of synchronous voltage activation maps shown in Fig. 4 (Bottom), in which a $\Delta t = 8\,ms$ lasts from one frame to the next on both surfaces. In the comparison, an intramural propagation delay, of the order of $10\,ms$, can be measured between ENDO and EPI activations, however the resulting propagating waves assume a close CV.

The recorded CVs resulted in general higher than the usual values reported in Literature [50]. However, the measurements are in the physiological range for canine heart velocities [51–53]. All our conduction velocity measurements were obtained from waves initiated at the edge of the free wall and propagated perpendicular to the thickness of the right ventricle and were measured on the epicardium and the endocardium simultaneously. In all cases electrical waves from the epicardium and endocardium traveled as a single wave front, and effects from pectinate muscle and purkinje fibers were minimum and not observed. The use of fluorescence optical mapping techniques adopted in the present work has been widely validated in the last two decades for restitution, wave propagation and CV measurements [49, 54–56] and give good agreement with micro-electrode recordings despite small errors in the signal due to optical scattering and absorption in tissue [44, 50, 57–63].

We further investigated the accuracy of the proposed measurements by evaluating the percentage of CV decrement during progressive CL fastening and for different thermal baths. In particular, by comparing the CV values in the range of the slowest and fastest CLs tested, we found that at $T = 40$°C there is no significant difference, while CV decreases 11% at $T = 37$°C, 40% at $T = 33$°C, 56% at $T = 29$°C, and 50% at $T = 26$°C. This large reduction in CV restitution substantially decreases the velocity of propagating waves. From the modeling point of view the thermal dependent functions mostly responsible for such a behavior are the $\eta(T)$ ones, which multiply the ionic current functions. Thus lowering $\eta_s$ results in lowering the CV by decreasing the sodium conductance on the wave front.

In Fig. 4 (Top right) we highlight the experimental alternans onset and conduction block as function of temperature. While a conduction block has to be synchronous between ENDO and EPI surfaces alternans onset is very different as the dynamics of the wave back between the epicardium and endocardium can be different, in particular the endocardial layer resulted more sen-

sitive to supporting alternating events at lower CLs: at the lowest measured temperature, $T = 26°C$, alternans is already present on the ENDO for CL $= 1000\,ms$ while it appears on the EPI only for CL $= 580\,ms$. However, for both surfaces, during progressive reduction of the pacing period we observe the increase of the minimum pacing cycle length which induces the onset of alternans in tissue as temperature decreases. An explanation for such a separation could be due to difference in electrophysiology between the epicardial and endocardial cells.

Our model is able to correctly reproduce with sufficient accuracy the occurrence of the conduction block in terms of CLs. However, by applying the criterion of Nolasco & Dahlen [64] for the prediction of alternans onset depending on the slope of the restitution curves (comparison of the slope of the curves with respect to the unitary diagonal slope $APD = DI$ as quantified in Fig. 2), the difference with the experimental data is much higher. In particular we observed cases of flat restitution curves especially for the case of hyperthermia ($T = 40°C$). However the Nolasco & Dahlen criteria is only valid for one dimensional maps. It is well known that the APD restitution is a multidimensional manifold [65–69] and when other effects such as memory, tissue heterogeneity and complex calcium dynamics are considered, alternans could appear even in relatively flat restitutions [49]. However these are not a target of the present work. In the next Section we will address the problem of prediction and evolution of alternans dynamics from a different perspective highlighting the role of temperature.

## C. Bifurcation Dynamics on a Ring

We further implemented the MM model on a 1D circuit with a single AP propagating wave. The minimum circuit length (or the equivalent pacing cycle length (CL)) for sustained AP propagation was found by analogy with sustained reentries during tachyarrhythmias. Therefore, by imposing a progressive circuit length reduction, more complex dynamics appeared. In particular, the maximum circuit length for discordant alternans onset and the minimum circuit length at which conduction block occurs present a strong variation with temperature. Figure 5 demonstrates the onset and amplitude of alternans (defined according to Eq. 18) at different temperatures through a bifurcation diagram built during progressive circuit length reduction. The absolute maximum and minimum APD with respect to circuit length for both ENDO and EPI are shown. The curves start at the minimum circuit length allowing sustained rotations without alternans and end when auto-annihilation arise, i.e. conduction block.

As a consequence of the different AP shapes and restitution curves modeled on experimental bases (See Fig. 2), differences can be noted between ENDO and EPI patterns: (1) epicardium presents shorter stabilization periods than endocardium at every tested temperature in

the 10°C range; (2) alternans onset does not correspond to the same circuit length between the two layers, i.e. it is not synchronous; (3) the modeled lengths are in agreement with the physiological values for sustained reentries, which reduces at higher temperatures; (4) the progressive reduction of the temperature gives rise to more enhanced alternans represented by a higher bifurcation amplitude; (5) at $T = 26°C$, due to the pronounced sigmoidal shape of the restitution curve, on the endocardial surface the bifurcation diagram is able to rejoin before conduction block occurs [70]. Moreover, the proposed analysis is able to demonstrate the effect of temperature during hyperthermia, i.e. $T = 40°C$, leading to a well defined alternating regime for both surfaces and appearing for smaller reentry circuits.

Most of these observations are in agreement with the experimental results, however alternans onset synchronization between ENDO and EPI is not correctly reproduced because of the discrepancy with the standard cobweb maps theory [64, 71, 72]. From the experimental point of view, however, the pacing electrode has been applied on the endocardial surface only, therefore these differences could be motivated by such a choice.

Finally we point out the range of circuit lengths from 6 to 18 $cm$ can more than double in length for a 10°C increase. Such a variation should be carefully taken into account and further investigated for arrhythmic events during heart surgery or defibrillating devices as well. In fact, the physical length for sustained alternating dynamics could be used for a more efficient arrhythmias termination depending on the thermal setup considered.

## D. Tissue Dependent Dynamics

Figure 6 shows the dynamics of the AP during large gradients of depolarization resulting from discordant alternans (spatial regions alternating in opposite phase) [18, 73, 74]. During discordant alternans the duration of action potential can vary between a long and a very short action potential in consecutive beats, therefore the shape of the propagating wave can vary substantially from one beat to the following. In order to obtain a short APD following a long one, the plateau of the propagating AP needs to suffer a collapse of the wave back in the center, which can be very abrupt during large alternans regimes. Such a phase wave can result on one or multiple non propagating waves left behind depending on the number of nodes (non-alternating regions) present in the tissue [79]. The darker line reported in Fig. 6, represents the AP at the time where this "droplet" wave is created for both the simulation and the experiment. This "droplet" wave can not propagate as it is formed by two wave backs. Therefore at some point in time along the cable it exists one wave front, or trigger wave and three wave backs or phase waves. The simulation and experiment show how discordant alternans produces a very large dispersion on the AP dynamics and can be a major cause towards an

arrhythmic state.

## IV.    DISCUSSION

Since thermal effects on biological tissues are often associated with severe sickness [75, 76] and sudden cardiac death [77], understanding the nonlinear mechanisms of their interaction with excitable media is of crucial importance in the medical practice. Although previous theoretical and experimental studies have discussed the role of fast cardiac pacing in relation with alternans onset, arrhythmias initiation and termination in normothermal conditions [78], we have argued in this work that such a mechanisms, here experimentally observed and numerically simulated, are dependent on the thermal setup considered. We suggest that assessment of clinically measured temperature values during surgery may help in the analysis and treatment of arrhythmias.

### A.    Novel Results

In this work we have presented a methodology to account for physiological changes due to temperature applying it to a phenomenological model of cardiac dynamics. The modified model, while relatively simple, successfully reproduces most of the phenomena obtained from experiments including increase in action potential duration, alternans regime, dispersion and decrease in conduction velocity as temperature decreases. It is further able to compare the synchrony or the delay of propagating action potential waves on both endocardial and epicardial layers, as well as the averaged restitution curves. Such a methodology can be similarly applied to generic RD systems of excitable media [32] or to more complex models [24], for further studies of thermal effects on arrhythmias.

The strong variation of APD and conduction velocity due to temperature is of great importance on the overall alternans dynamics and would deserve more attention from both the experimental and modeling point of view. We demonstrated that in the hypothermic regime, $T = 26°C$, the sigmoidal shape of the restitution curves in the endocardial case (without considering splitting) gives rise to a rejoining of the bifurcation diagram during progressive reduction of the circuit length, thus leading to alternans disappearance before conduction block occurrence. Such a phenomena is not observed on the epicardial layer, thus highlighting the strongly nonlinear character of the model. Moreover, in the hyperthermic regime, $T = 40°C$, definite alternans exist and appear for shorter circuit lengths on both surfaces. These observations explain the arrhythmic risk in both regimes, leading to the necessity of a careful control of pathologic thermal states, eventually arising from open heart surgery, inflammations or fever.

### B.    One wave front, multiple wave backs.

We have shown experimentally for the first time the existence of traveling waves with one wave front and multiple wave backs as previously predicted by numerical simulations [79]. The existence of multiple wave backs are necessary for the tissue to allow regions of large APD next to regions with small APD so while the activation has finished in one portion of the tissue, another region needs to remain activated. While there could be only one wave front, the number of wave backs behind the front will depend on the number of nodal lines during discordant alternans in the tissue. The number of nodal lines in a tissue is a function of the diffusion and coupling in the tissue [80].

### C.    Limitations & Future Perspectives

A limitation of the present study can be recognized in the range of temperature covered [26 to 40]°C. A finer tuning of the model parameters could increase this range, however a better fitting of the experimental data would require the description of every single parameter as function of temperature. Such an approach, if feasible from a theoretical point of view, does not gain any chance of applicability due to the tremendous increase of parameters, and lacks of flexibility. A better understanding of the recovery dynamics via a kinetic based formulation, on the other hand, would help the overall comprehension of the highly nonlinear behaviors observed and their interaction with temperature. The introduction of temperature changes on single gap junction formulations would translate the present model into a multiscale approach, that is not considered in this work.

In the present study we only considered averaged restitution curves, however it would be of great interest also to take into account the presence of restitution curve splitting from both the experimental and modeling point of view. In this direction, short-memory feedback [81] and intracellular calcium handling would improve the actual modeling approach toward reacher and more realistic alternans dynamics. It is well known the mutual feedback between cardiac action potential, that controls the rise and fall of intracellular free calcium and the excitation-contraction coupling, and the reverse process due to calcium-dependent ionic currents [82]. The latter has been implicated as the mechanism underlying several arrhythmias and heart diseases. However, at very fast pacing cycle lengths (i.e. less than $200\,ms$), it has been shown that intracellular calcium and membrane voltage present a significant delay. The current research on dual calcium/voltage optical mapping technique and the study of their mutual information due to photon scattering is still under investigation [63]. The overall effects are not yet fully explored and their possible uncoupling during fast pacing or ventricular fibrillation is still debated. These effects, together with the presence of tissue

anisotropy and heterogeneity would motivate then the occurrence of alternans even when the slopes of the restitution branches are less than one [49], as shown in the present work.

Temperature affects also the mechanical characters of biological excitable media. In particular, lower temperatures induce electromechanical changes in the heart mainly due to the accumulation of intracellular calcium concentration [83], thus leading to the consequent APD increase, developed force, and alternans onset. Also in this case, intracellular calcium handling instabilities would be of great importance for a complete cellular based analysis of the complex phenomena here discussed. However few mathematical models have been developed in this direction. On such a basis, it would be very useful

a full coupled thermo-electro-mechanic approach in order to theoretical validate recent defibrillating techniques in the low energy regime [28, 29, 41, 48, 84]. Finally, the proposed approach would be of great interest also for related problems addressing excitable RD media, i.e. intestine [85], brain [14, 76, 86] and chemical systems [87].

## D. Acknowledgment

[1] A.T. Winfree, *When Time Breaks Down: The Three-Dimensional Dynamics of Electrochemical Waves and Cardiac Arrhythmias*, Princeton University Press., (1987).

[2] A.T. Winfree, *The Geometry of Biological Time*, Springer-Verlag, (2001).

[3] D. Bini, C. Cherubini, S. Filippi, A. Gizzi, and P.E. Ricci, *Commun. Comput. Phys.* **8**, 610 (2010).

[4] J.M. Davidenko, A.V. Pertsov, R. Salomonsz, W. Baxter, and J. Jalife, *Nature* **355**, 349 (1992).

[5] E.M. Cherry, and F.H. Fenton, *New J. Phys.* **10**, 125016 (2008).

[6] C. Luengviriya, J. Luengviriya, M. Sutthiopad, and S.C. Müller, *IPCBEE*, **38**, 105–109 (2012)

[7] A.C. Guyton, and J.E. Hall, *Textbook of Medical Physiology, 10th Ed.*, W.B. Saunders Company, (2000).

[8] B.P. McDermott, D.J. Casa, M.S. Ganio, R.M. Lopez, S.W Yeargin, L.E. Armstrong, C.M. Maresh, *Journal of Athletic Training* **44**, 84–93 (2009).

[9] K.H. Polderman, *The Lancet* **371**, 1955 (2008).

[10] L.G.C.E. Pugh, *Brit. Med. J.*, **2**, 333–337 (1967).

[11] E.L. Lloyd, *Hypothermia and Cold Stress*, Chapman and Hall, (1986).

[12] G.G. Giesbrecht, *Aviat. Space Environ. Med.*, **71**, 733–752 (2000).

[13] M. Gilbert, R. Busund, A. Skagseth, P.A. Nilsen, J.P. Solbø, *Lancet* **355**, 375–376 (2000).

[14] E. Kochs, *J. Neurosurg. Anesthesiol.* **7**, 222–228 (1995).

[15] H. Bjørnstad, P.M. Tande, D.A. Lathrop, and H. Refsum, *Card. Res.* **27**, 946 (1993).

[16] T. Kiyosue, M. Arita, H. Mutamatsu, A.J. Spindler, and D. Noble, *J. Physiol.* **468**, 85 (1993).

[17] W.J. Crozier, *J. Gen. Physiol.* **9**, 531 (1926).

[18] J.M. Pastore, S.D. Girouard, K.R. Laurita, F.G. Akar, and D.S. Rosenbaum, *Circulation* **99**, 1385 (1999).

[19] M. Watanabe, N.F. Otani, R.F. Gilmour, Jr., *Circ. Res.* **76**, 915 (1995).

[20] Z. Qu, J.N. Weiss, and A. Garfinkel, *Phys. Rev. Lett.* **78**, 1387 (1997).

[21] M.A. El-Brawany, D.K. Nassiri, G. Terhaar, A. Shaw, I. Rivens, and K. Lozhken, *J. Med. Eng. Tech.* **33**, 249 (2009).

[22] A.V. Glukhov, Y.V. Egorov, I.R. Efimov, and L.V. Rosenshtraukh., *Living in a Seasonal World* T. Ruf et al. (eds.) (2012).

[23] A.L. Hodgkin, and A.F. Huxley, *J. Physiol.* **117**, 500 (1952).

[24] F.H. Fenton, and E.M. Cherry, *Scholarpedia* **3**, 1868 (2008).

[25] C. Cherubini, and S. Filippi *Phys. Rev. E* **80**, 046117 (2009).

[26] M.P. Nash, and A.V. Panfilov, *Prog. Biophys. Mol. Biol.* **85**, 501-522 (2004).

[27] D. Bini, C. Cherubini, and S. Filippi, *Phys. Rev. E* **72**, 041929 (2005).

[28] C. Cherubini, S. Filippi, P. Nardinocchi, and L. Teresi. *Prog. Biophys. Mol. Biol* **97**, 562–573 (2008).

[29] C. Cherubini, S. Filippi, P. Nardinocchi, and L. Teresi. *Mechanosensitivity of the Heart*, Springer Netherlands, (2010).

[30] D. Kondepudi, and I. Prigogine. *Modern Thermodynamics: From Heat Engines to Dissipative Structures*, John Wiley & Sons Ltd (2006).

[31] H.H. Pennes, *Journal of Applied Physiology* **1**, 93 (1948).

[32] A. Gizzi, C. Cherubini, S. Migliori, R. Alloni, R. Portuesi, and S. Filippi, *Phys. Biol.* **7**, 016011 (2010).

[33] T. Ashihara, N. Trayanova, K. Nakazawa, M. Yamazaki, H. Honjio, I. Sakuma, K. Kamiya and I. Sakuma, *Heart Rhythm* **2**, 5 (2005).

[34] D. Bini, C. Cherubini, and S. Filippi, *Phys. Rev. E* **74**, 041905 (2006).

[35] D. Bini, C. Cherubini, and S. Filippi, *Chaos* **42**, 2057–2066 (2009).

[36] R.H. Clayton, O. Bernus, E.M. Cherry, H. Dierckx, F.H. Fenton, L. Mirabella, A.V. Panfilov, F.B. Sachse, G. Seemann, and H. Zhang, *Prog. Biophys. Mol. Biol.* **104**, 22 (2011).

[37] A. B.-Orovio, E.M. Cherry, and F.H. Fenton. *J. Theor. Biol.* **253**, 544 (2008).

[38] J.W. Moore, *Fed. Proc.* **17**, 113 (1958).

[39] M. Courtemanche, L. Glass, and J.P. Keener, *Phys. Rev. Lett.* **70**, 2182 (1993).

[40] L. Glass, and M.E. Josephson, *Phys. Rev. Lett.* **75**, 2059 (1995).

[41] S. Luther, F.H. Fenton, B.G. Kornreich, A. Squires, P. Bittihn, D. Hornung, M. Zabel, J. Flanders, A. Gladuli,

L. Campoy, et. al., *Nature* **13**, 235 (2011).

[42] F.H. Fenton, S. Luther, E.M. Cherry, N.F. Otani, V. Krinsky, A. Pumir, E. Bodenschatz, and R.F. Gilmour, Jr., *Circulation* **120**, 467–476 (2009).

[43] A.V. Glukhov, V.V. Fedorov, Q. Lou, V.K. Ravikumar, P.W. Kalish, R.B. Schuessler, N. Moazami, and I.R. Efimov, *Circ. Res.* **106**, 981–991 (2010).

[44] C. Cabo, A.M. Pertsov, W.T. Baxter, J.M. Davidenko, R.A. Gray, and J. Jalife, *Circ. Res.* **75**, 1014–1028 (1994).

[45] M.W. Kay, and R.A. Gray, *IEEE Trans. Biomed. Eng.* **52**, 50-63 (2005).

[46] F. Qu, C.M. R. Vladimir, P. Nikolski, C. Grimm, and I.R. Efimov, *J. Biomed. Optics.***12**, 044019 (2007).

[47] S.A. Niederer, E. Kerfoot, A.P. Benson, M.O. Bernabeu, O. Bernus, C. Bradley, E.M. Cherry, R. Clayton, F.H. Fenton, A. Garny, et. al., *Philos Transact A Math Phys Eng Sci.* **369**, 4331–4351 (2011).

[48] C. Cherubini, S. Filippi, and A. Gizzi, *Phys. Rev. E* **85**, 031915 (2012).

[49] E.M. Cherry, and F.H. Fenton. *Am. J. Physiol. Heart Circ. Physiol.* **292**, H43–H45 (2007).

[50] I. Banville, and R.A. Gray, *J. Cardiovasc. Electrophysiol.* **13**, 1141–1149, (2002).

[51] S. Rohr, *Cardiovasc. Res.* **62**, 309–322, (2004).

[52] F.G. Akar, R.D. Nass, S. Hahn, E. Cingolani, M. Shah, G.G. Hesketh, D. DiSilvestre, R.S. Tunin, D.A. Kass, and G.F. Tomaselli, *Am. J. Physiol. Heart Circ. Physiol.* **293**, H1223–H1230, (2007).

[53] K.F. Decker, J. Heijman, J.R. Silva, T.J. Hund, and Y. Rudy, *Am. J. Physiol. Heart. Circ. Physiol.* **296**, H1017–H1026 (2009). *Neurobiol. Dis.* **41**, 655–660 (2011).

[54] J.I. Laughner, F.S. Ng, M.S. Sulkin, M.A. Arthur, and I.R. Efimov. *Am. J. Physiol. Heart Circ. Physiol.* **303**, H753–765 (2012).

[55] I.R. Efimov, and G. Salama, *Circ. Res.* **110**, e70–71 (2012).

[56] S. Mironov, J. Jalife, and E.G. Tolkacheva. *Circulation* **118**, 17–25 (2008).

[57] Y. Asano, J.M. Davidenko, W.T. Baxter, R.A. Gray, and J. Jalife, *JACC* **29**, 831–42 (1997).

[58] R.A. Gray, A.M. Pertsov, and J. Jalife, *Nature* **392**, 75–78 (1998).

[59] M. Or-Guil, J. Krishnan, I.G. Kevrekidis, and M. Bär, *Phys. Rev. E* **64**, 046212 (2001).

[60] R.A. Gray, A. Iyer, O. Berenfeld, A.M. Pertsov, and C.J. Hyatt, *J. Electrocardiol.* **39**, S13–S18 (2006).

[61] S. Iravanian, and D.J. Christini, *Am. J. Physiol. Heart. Circ. Physiol .***293**, H2605–H2611 (2007).

[62] A.D. Bachtel, R.A. Gray, J.M. Stohlman, E.B. Bourgeois, A.E. Pollard, and J.M. Rogers, *IEEE Trans. Biomed. Eng.***58**, 2120–2126 (2011).

[63] M.J. Bishop, A. Rowley, B. Rodriguez, G. Plank, D.J. Gavaghan, and G. Bub, *Biophys. J.* **101**, 307-318 (2011).

[64] J.B. Nolasco, and R.W. Dahlen, *J. Appl. Physiol.* **25**, 191–196 (1968).

[65] E.M. Cherry, and F.H. Fenton, *Am. J. Physiol. Heart Circ. Physiol.* **286**, H2332–H2341 (2004).

[66] B. Echebarria, A. Karma *Phys. Rev. E.* **76**, 051911 (2007).

[67] D.J. Gauthier, and J.E.S. Socolar, *Phys. Rev. Lett.* **79**, 4938–4938 (1997)

[68] G.M Hall, S. Bahar, and D.J. Gauthier, *Phys. Rev. Lett.* **82**, 2995–2998 (1999).

[69] G.M Hall, and D.J. Gauthier, *Phys. Rev. Lett.* **88**, 198102 (2002).

[70] F.H. Fenton, E.M. Cherry, H.M. Hastings, and S.J. Evans *Chaos* **12**, 852–892 (2002).

[71] S.H. Strogatz, *Nonlinear Dynamics And Chaos: With Applications To Physics, Biology, Chemistry, And Engineering*, Westview Press (2001).

[72] F.H. Fenton, E.M. Cherry, H.M. Hastings, and S.J. Evans *Biosystems.* **64**, 73–96 (2002).

[73] M.A. Watanabe, F.H. Fenton, S.J. Evans, H.M. Hastings, and A. Karma, *J. Cardiovasc. Electrophysiol.* **12**, 196–206 (2001).

[74] Z. Qu, A. Garfinkel, P.-S. Chen, and J.N. Weiss, *Circulation.* **102**, 1664–1670 (2000).

[75] A. Burashnikov, W. Shimizu, and C. Antzelevitch, *Circ. Arrhythm. Electrophysiol.* **1**, 202 (2008).

[76] N.A. Hawkins, M.S. Martin, W.N. Frankel, J.A. Kearney, and A. Escay,

[77] S. Modi, and A.D. Krahn, *Circulation* **123**, 2994 (2011).

[78] Y. Nagai, H. González, A. Shrier, and L. Glass, *Phys. Rev. Lett.* **84**, 4248 (2000).

[79] F.H. Fenton, E.M. Cherry, and L. Glass, *Scholarpedia* **3**, 1665 (2008).

[80] W.-J. Rappel, F.H. Fenton, and A. Karma *Phys. Rev. Lett.* **83**, 456–459 (1999).

[81] I. Banville, N. Chattipakorn, and R.A. Gray, *J. Cardiovasc. Electrophysiol.* **15**, 455–463, (2004).

[82] G. Salama, and S.M. Hwang, *Curr. Protoc. Cytom.* **49** 1–32 (2009).

[83] H. Bjørnstad, D.A. Lathrop, and H. Refsum, *Card. Res.* **28**, 55–60 (1994).

[84] A. Pumir, S. Sinha, S. Sridhar, M. Argentina, M. Horning, S. Filippi, C. Cherubini, S. Luther, and V. Krinsky, *Phys. Rev. E* **81**, 010901(2010).

[85] A. Altomare, M.P.L. Guarino, A. Gizzi, S. Cocca, C. Cherubini, R. Alloni, S. Filippi, and M. Cicala, *Gastroenterology*, **142**, S608–S609 (2012).

[86] J. Zaremba, *Med. Sci. Monit.* **10**, 148-153 (2004).

[87] Z.A. Jiménez, and O. Steinbock, *Phys. Rev. Lett.* **109**, 098301 (2012).

## Appendix

In Tab. 1 the model parameters are reported distinguishing between endocardium and epicardium layers for the two thermal ranges, [29; 40]°C and $T = 26$°C. In Tab. 2 and 3 the fitting parameters of the experimental restitution values are reported, adopting the MATLAB CFTOOL toolboxes *smoothing spline* and *polynomial*, respectively. The parameters $p$, user defined, are reported in the first case. In the second case the polynomial coefficients are given and the R-square goodness of the fit is reported in both cases. The general form of the *polynomial* fitting curve adopted is: $\sum_{i=1}^{7} c_i x^{7-i}$. $ENDO_{26}$ and $EPI_{26}$ values are fitted by linear piecewise interpolating curves (not reported).

Tab.1. Model parameters for epicardial and endocardial action potential MM formulation, effective $Q_{10}$ and Moore thermal factors. Units are given in $ms, cm, mV, mS, \mu F, g, °C$.

| $\text{EPI}_{29-40}$ | $\text{ENDO}_{29-40}$ | $\text{EPI}_{26}$ | $\text{ENDO}_{26}$ |
|---|---|---|---|
| $u_o = 0$ | $u_o = 0$ | $u_o = 0$ | $u_o = 0$ |
| $u_u = 1.55$ | $u_u = 1.56$ | $u_u = 1.55$ | $u_u = 1.56$ |
| $\theta_v = 0.3$ | $\theta_v = 0.3$ | $\theta_v = 0.3$ | $\theta_v = 0.3$ |
| $\theta_w = 0.13$ | $\theta_w = 0.13$ | $\theta_w = 0.13$ | $\theta_w = 0.13$ |
| $\theta_v^- = 0.006$ | $\theta_v^- = 0.2$ | $\theta_v^- = 0.006$ | $\theta_v^- = 0.2$ |
| $\theta_o = 0.006$ | $\theta_o = 0.006$ | $\theta_o = 0.006$ | $\theta_o = 0.006$ |
| $\tau_v^+ = 1.4506$ | $\tau_v^+ = 1.4506$ | $\tau_v^+ = 1.4506$ | $\tau_v^+ = 1.4506$ |
| $\tau_{v1}^- = 20$ | $\tau_{v1}^- = 55$ | $\tau_{v1}^- = 10$ | $\tau_{v1}^- = 15$ |
| $\tau_{v2}^- = 1150$ | $\tau_{v2}^- = 40$ | $\tau_{v2}^- = 1150$ | $\tau_{v2}^- = 40$ |
| $\tau_{w1}^- = 120$ | $\tau_{w1}^- = 40$ | $\tau_{w1}^- = 75$ | $\tau_{w1}^- = 40$ |
| $\tau_{w2}^- = 300$ | $\tau_{w2}^- = 115$ | $\tau_{w2}^- = 90$ | $\tau_{w2}^- = 165$ |
| $\tau_{w1}^+ = 120$ | $\tau_{w1}^+ = 175$ | $\tau_{w1}^+ = 90$ | $\tau_{w1}^+ = 175$ |
| $\tau_{w2}^+ = 140$ | $\tau_{w2}^+ = 230$ | $\tau_{w2}^+ = 140$ | $\tau_{w2}^+ = 150$ |
| $k_w^- = 65$ | $k_w^- = 20$ | $k_w^- = 65$ | $k_w^- = 8000$ |
| $u_w^- = 0.03$ | $u_w^- = 0.00615$ | $u_w^- = 0.02$ | $u_w^- = 0.005$ |
| $k_w^+ = 5.7$ | $k_w^+ = 8$ | $k_w^+ = 6.5$ | $k_w^+ = 8$ |
| $u_w^+ = 0.15$ | $u_w^+ = 0.0005$ | $u_w^+ = 0.8$ | $u_w^+ = 0.0005$ |
| $\tau_{fi} = 0.11$ | $\tau_{fi} = 0.10$ | $\tau_{fi} = 0.11$ | $\tau_{fi} = 0.10$ |
| $\tau_{o1} = 400$ | $\tau_{o1} = 470$ | $\tau_{o1} = 400$ | $\tau_{o1} = 470$ |
| $\tau_{o2} = 6$ | $\tau_{o2} = 6$ | $\tau_{o2} = 6$ | $\tau_{o2} = 6$ |
| $\tau_{so1} = 30.0181$ | $\tau_{so1} = 40$ | $\tau_{so1} = 30.0181$ | $\tau_{so1} = 40$ |
| $\tau_{so2} = 0.9957$ | $\tau_{so2} = 1.2$ | $\tau_{so2} = 0.9957$ | $\tau_{so2} = 1.2$ |
| $k_{so} = 2.0458$ | $k_{so} = 2$ | $k_{so} = 2.0458$ | $k_{so} = 2$ |
| $u_{so} = 0.65$ | $u_{so} = 0.65$ | $u_{so} = 0.65$ | $u_{so} = 0.65$ |
| $\tau_{s1} = 2.7342$ | $\tau_{s1} = 2.7342$ | $\tau_{s1} = 2.7342$ | $\tau_{s1} = 2.7342$ |
| $\tau_{s2} = 16$ | $\tau_{s2} = 2$ | $\tau_{s2} = 16$ | $\tau_{s2} = 2$ |
| $k_s = 2.0994$ | $k_s = 2.0994$ | $k_s = 2.0994$ | $k_s = 2.0994$ |
| $u_s = 0.9087$ | $u_s = 0.9087$ | $u_s = 0.9087$ | $u_s = 0.9087$ |
| $\tau_{si} = 1.8875$ | $\tau_{si} = 2.9013$ | $\tau_{si} = 1.8875$ | $\tau_{si} = 2.9013$ |
| $\tau_{w\infty} = 0.07$ | $\tau_{w\infty} = 0.0273$ | $\tau_{w\infty} = 0.07$ | $\tau_{w\infty} = 0.0273$ |
| $w_\infty^* = 0.94$ | $w_\infty^* = 0.78$ | $w_\infty^* = 0.94$ | $w_\infty^* = 0.78$ |
| $Q_{10,v} = 1.5$ | $Q_{10,v} = 1.5$ | $Q_{10,v} = 0.9$ | $Q_{10,v} = 1.5$ |
| $Q_{10,w} = 2.45$ | $Q_{10,w} = 2.45$ | $Q_{10,w} = 3$ | $Q_{10,w} = 2.5$ |
| $Q_{10,s} = 1.5$ | $Q_{10,s} = 1.5$ | $Q_{10,s} = 1.35$ | $Q_{10,s} = 1.5$ |
| $A_{fi} = 1$ | $A_{fi} = 1$ | $A_{fi} = 2$ | $A_{fi} = 1.5$ |
| $B_{fi} = 0.065$ | $B_{fi} = 0.065$ | $B_{fi} = 0.065$ | $B_{fi} = 0.065$ |
| $A_{so} = 1$ | $A_{so} = 1$ | $A_{so} = 1.4$ | $A_{so} = 1$ |
| $B_{so} = 0.008$ | $B_{so} = 0.008$ | $B_{so} = 0.008$ | $B_{so} = 0.008$ |
| $A_{si} = 1$ | $A_{si} = 1$ | $A_{si} = 1.4$ | $A_{si} = 1$ |
| $B_{si} = 0.008$ | $B_{si} = 0.008$ | $B_{si} = 0.008$ | $B_{si} = 0.008$ |

Tab.2. Fitted curve (smoothing spline). Parameters and Statistic.

| Curve | $p$ | R-square |
|---|---|---|
| $\text{ENDO}_{29}$ | $2.3730462 \cdot 10^{-5}$ | $0,9991$ |
| $\text{ENDO}_{33}$ | $4.7727621 \cdot 10^{-4}$ | $0,9987$ |
| $\text{EPI}_{29}$ | $1.1400597 \cdot 10^{-4}$ | $0,9956$ |
| $\text{EPI}_{33}$ | $4.2275630 \cdot 10^{-4}$ | $0,9989$ |
| $\text{EPI}_{40}$ | $1.6385054 \cdot 10^{-4}$ | $0,9988$ |

Tab.3. Fitted curve (polynomial). Parameters and Statistic.

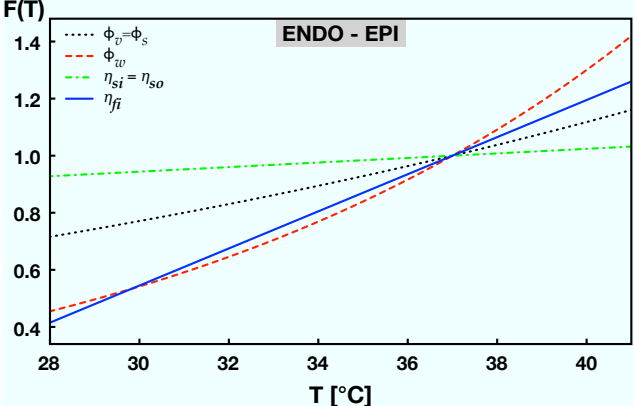| Curve | $c_1$ | $c_2$ | $c_3$ | $c_4$ | $c_5$ | $c_6$ | $c_7$ | R-square |
|---|---|---|---|---|---|---|---|---|
| $\text{ENDO}_{37}$ | $0$ | $0$ | $0$ | $3.12 \cdot 10^{-6}$ | $-3.683 \cdot 10^{-3}$ | $1,306$ | $33,75$ | $0,9953$ |
| $\text{ENDO}_{40}$ | $-1.759 \cdot 10^{-14}$ | $4.83 \cdot 10^{-11}$ | $-5.279 \cdot 10^{-8}$ | $2.946 \cdot 10^{-5}$ | $-9.076 \cdot 10^{-3}$ | $1,604$ | $19,86$ | $0,9995$ |
| $\text{EPI}_{37}$ | $0$ | $0$ | $-1.946 \cdot 10^{-8}$ | $1.958 \cdot 10^{-5}$ | $-7515 \cdot 10^{-3}$ | $1,481$ | $33,69$ | $0,998$ |

FIG. 1: (Color online) Temperature dependent factors variations according to the analytical expressions reported in Eq. 16, 17. The thermal range spans over $10°$C as stated by the thermodynamical assumptions. Endocardial and epicardial surfaces have been assigned the same numerical values in the thermal range $[29, 40]°$C (see Tab.1).
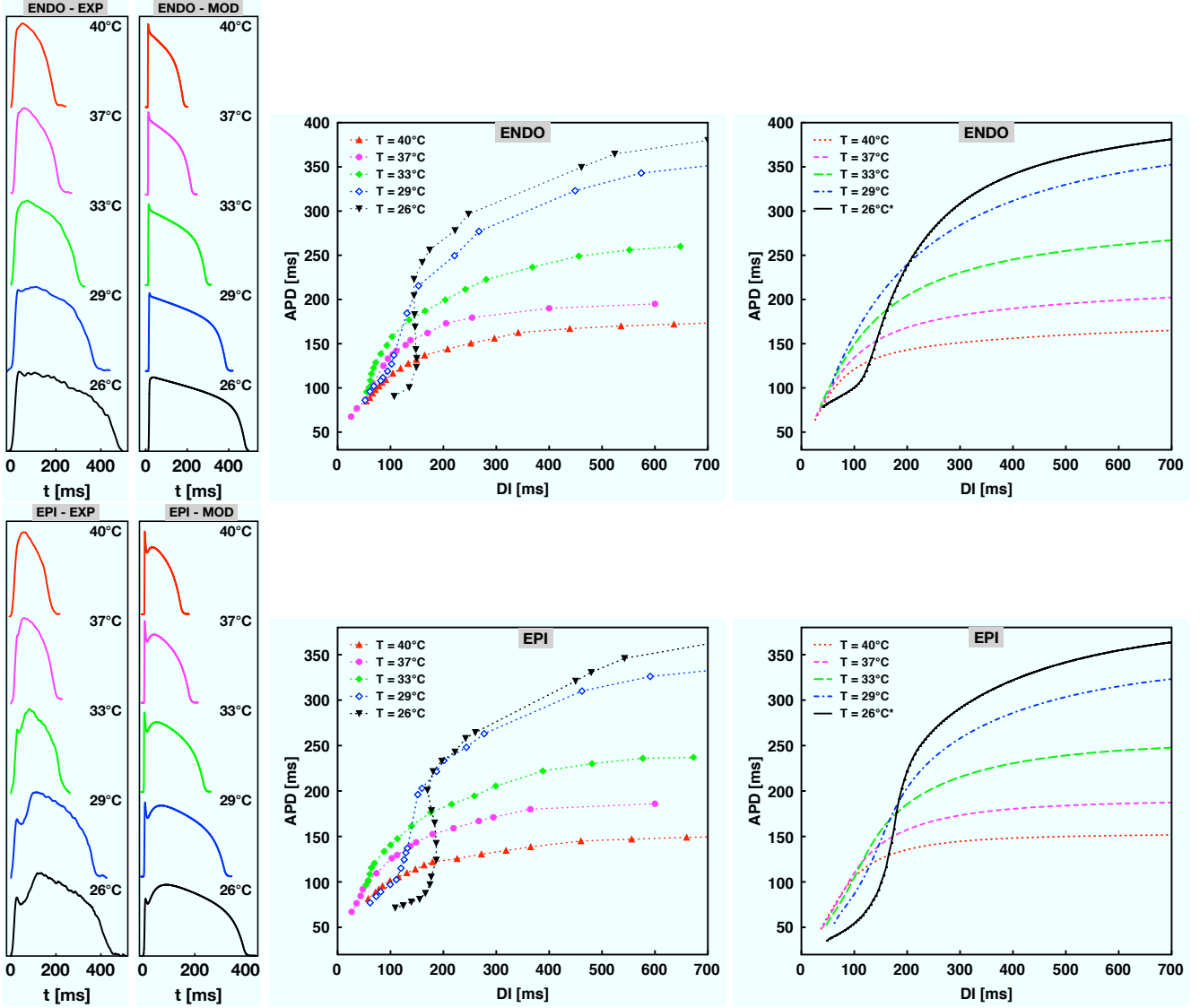
FIG. 2: (Color online) Endocardial (up) and epicardial (down) experimental (left) vs. modeled (right) action potential shapes (fixed maximum CL) and APD-DI restitution curves at five different temperatures. Lowering the temperature the restitution curves shift up; for temperatures below 29°C APD grows at long pacing periods but dramatically decreases at shorter ones. The ENDO experimental restitution curves presented a slope $\geq 1$ for CL equal to: $65\,ms$ at $T = 40°$C, $90\,ms$ at $T = 37°$C, $105\,ms$ at $T = 33°$C, $160\,ms$ at $T = 29°$C, $180\,ms$ at $T = 26°$C. The EPI experimental restitution curves presented a slope $\geq 1$ for CL equal to: no CL at $T = 40°$C, $70\,ms$ at $T = 37°$C, $80\,ms$ at $T = 33°$C, $140\,ms$ at $T = 29°$C, $180\,ms$ at $T = 26°$C. The corresponding simulated restitution curves assume a similar trend of slope variation with temperature in good agreement with the experimental values (in the range of $10\,ms$ difference). The sigmoidal restitution shape at $26°$C, required an alternative set of parameters (See Tab.1). The error bars in the experimental restitution curves are of the order $\pm 4\,ms$ (not reported for clarity of the figure).
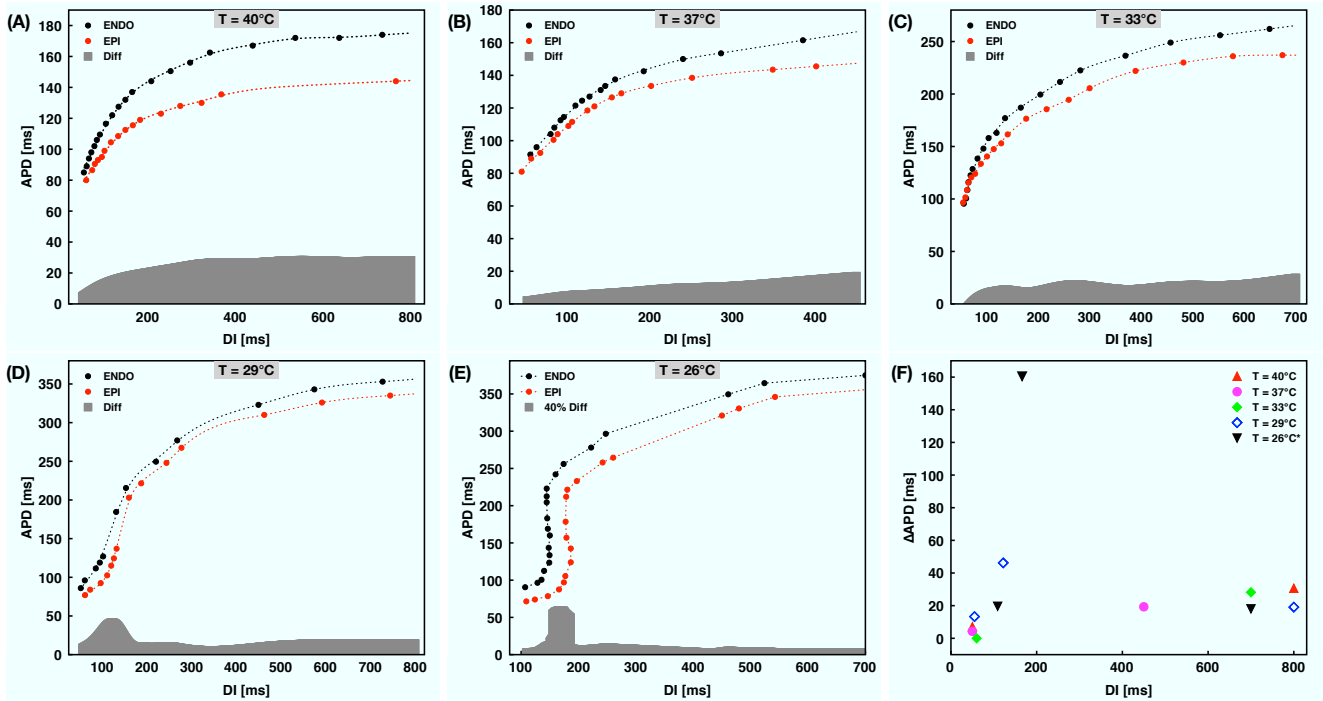
FIG. 3: (Color online) (A-E) Comparison of the synchronous restitution curves on the opposite surfaces for five different temperatures (ENDO black, EPI red). APD differences are reported as gray bars. At $T = 26°C$ the difference is scaled down in order to fit the graph. (F) Maximum and minimum APD differences collected at the highest and lowest CLs. For $T = 26, 29°C$, an intermediate value is shown corresponding to the inflection region of the sigmoidal curves. Fitting parameters are reported in Tab. 2 and 3.
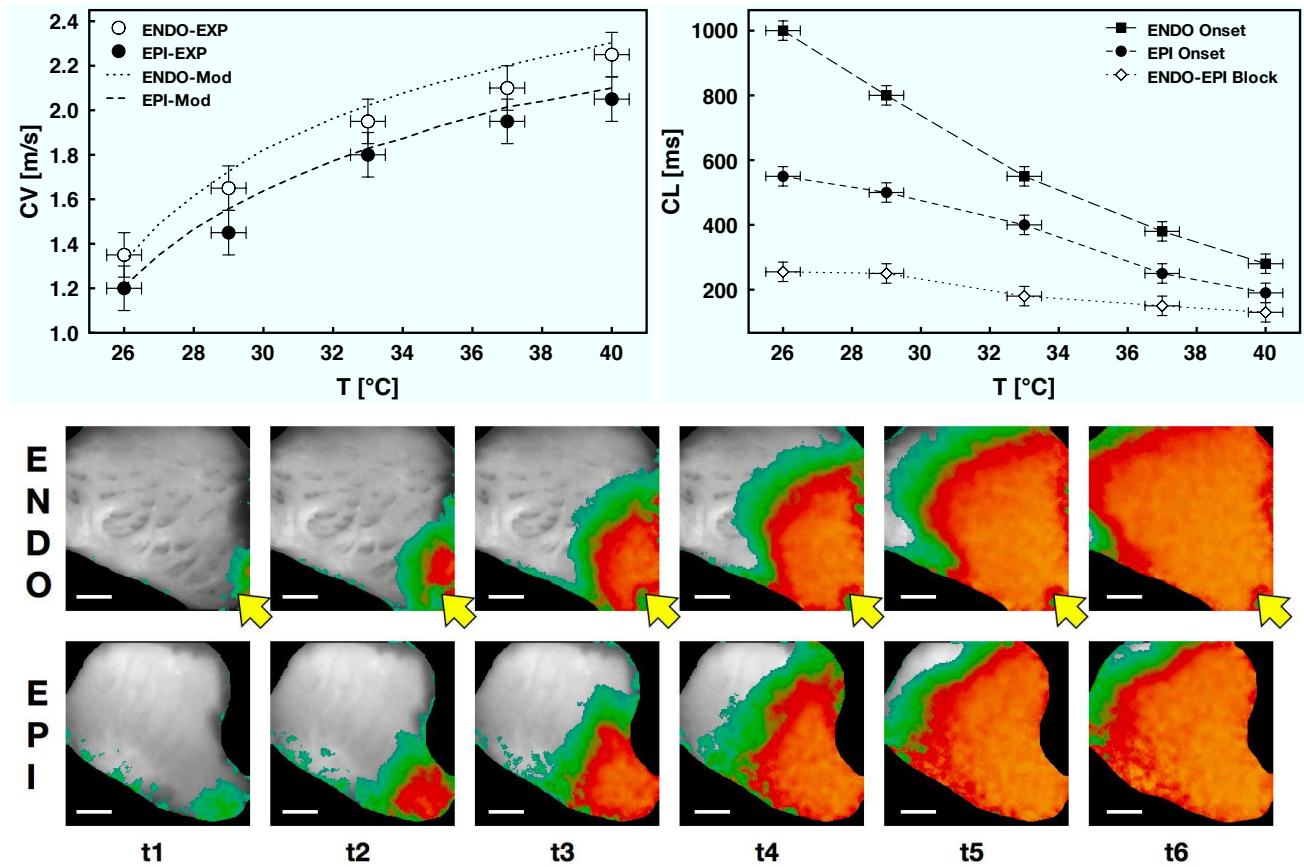
FIG. 4: (Color online) (Top left) Experimental vs. modeled conduction velocities as function of temperature (fixed maximum CL). Error bars are related to both CV, $\pm 0.3\,m/s$, and temperature, $\pm 0.5°$C, estimations. (Top right) Experimental alternans onset and conduction block as function of temperature during progressive reduction of the restitution pacing protocol on endocardium (filled square) and epicardium (filled circle). (Bottom) Endocardial (ENDO) and epicardial (EPI) activation voltage maps (color code refers to the AP propagating wave over imposed to the gray tissue structure) following endocardial electrical stimulation at CL $= 550\,ms$ (arrow for pacing electrode) at $T = 37°$C. The sequences of propagation last $8\,ms$ and a measurable difference in the propagating wave front is visible. A white length scale bar of $1\,cm$ is indicated.
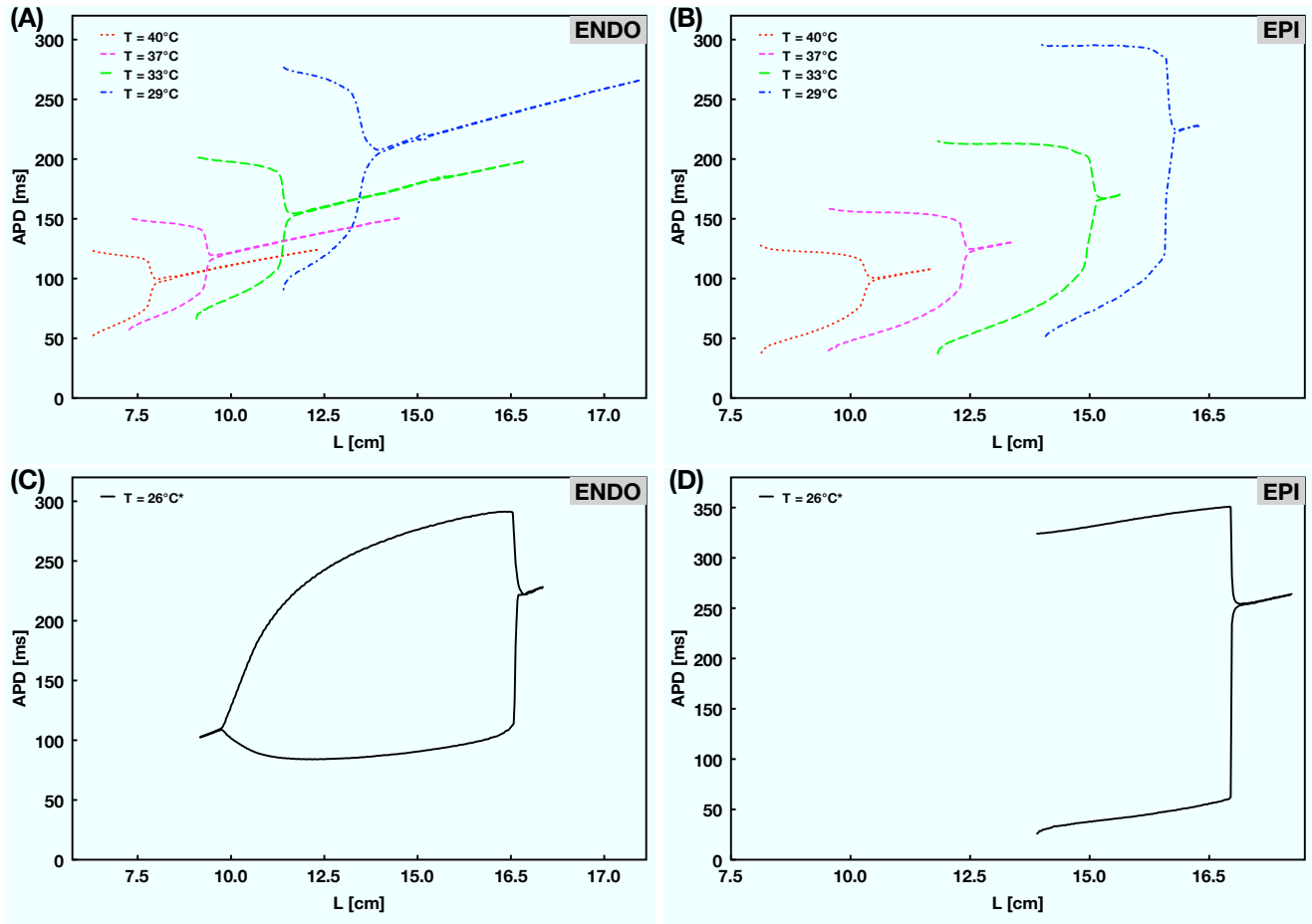
FIG. 5: (Color online) Endocardial (A, C) and epicardial (B, D) bifurcation diagrams obtained during circuit length reduction for five different temperatures. The modeled temperature $T = 26°C$ required an alternative set of parameters shown below (See Tab.1). The curves start at the minimum circuit length allowing sustained rotations at the different temperatures ending when auto-annihilation arise, i.e. conduction block. Measurable differences can be noted between ENDO and EPI patterns. The lowest temperature allows the bifurcation rejoining on the endocardial domain before conduction block occurrence.
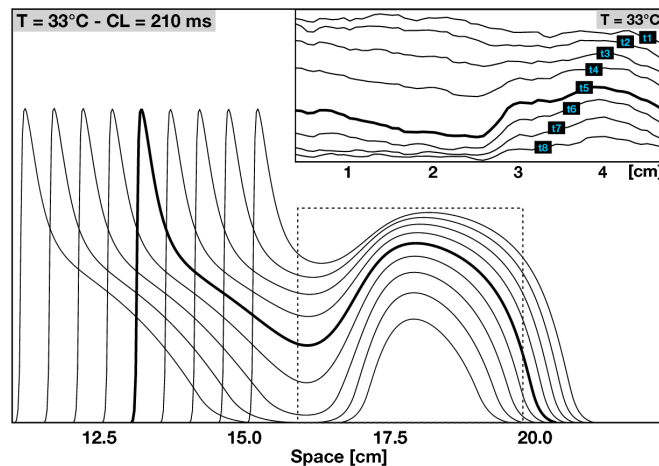


FIG. 6: (Color online) Simulated action potential propagation, during discordant alternans regime, for the model at $33°C$ and pacing cycle length of $210\,ms$. Nine equally spaced frames in time of an AP propagating from the right to the left show the complex dynamics of the wave back during discordant alternans. Similar sequence is presented from an experiment on the inset where the development of a "double" depolarization phase is shown at $33°C$. The darker signal identifies equivalent signals at a given time between the simulation and the experiment showing two out of the three wave backs produced by a single wave front.